International Journal of Chronic Obstructive Pulmonary Disease

Dovepress
Taylor & Francis Group

Open Access Full Text Article

ORIGINAL RESEARCH

Accurate Asthma-COPD Overlap Classification via Deep Transfer Learning in Medical Image Segmentation

Weijie Ye[1,*], Dieyi Mo[2,*], Yubin Yang[3]

[1]Department of Respiratory, Guangzhou Panyu District Maternal and Child Health Hospital (Affiliated Hospital Group of Guangdong Medical University Panyu HeXian Memorial Hospital), Guangzhou, People's Republic of China; [2]Department of Anesthesiology, Guangzhou Panyu District Maternal and Child Health Hospital (Affiliated Hospital Group of Guangdong Medical University Panyu HeXian Memorial Hospital), Guangzhou, People's Republic of China; [3]Department of Ophthalmology, Guangzhou Panyu District Maternal and Child Health Hospital (Affiliated Hospital Group of Guangdong Medical University Panyu HeXian Memorial Hospital), Guangzhou, People's Republic of China

*These authors contributed equally to this work

Correspondence: Yubin Yang, Department of Ophthalmology, Guangzhou Panyu District Maternal and Child Health Hospital (Affiliated Hospital Group of Guangdong Medical University Panyu HeXian Memorial Hospital), Guangzhou, People's Republic of China, Email ye206@163.com

Abstract: Differentiating asthma from chronic obstructive pulmonary disease (COPD) remains challenging in clinical practice, and asthma-COPD overlap (ACO) lacks universally accepted diagnostic criteria. In this study, we propose a chest computed tomography (CT) image segmentation framework based on deep transfer learning to support imaging-assisted ACO-related classification as a proof-of-concept approach. Experiments were performed in a single-center cohort of patients with asthma, COPD, and ACO. Model performance was evaluated using classification accuracy and segmentation Dice similarity coefficient against expert-annotated reference masks. In addition, lung function parameters, inflammatory biomarkers, and ACT/CAT scores were summarized to characterize cohort profiles and assist clinical interpretation; these variables were not predicted by the AI model. The proposed approach achieved the highest ACO classification accuracy (93.21%), outperforming NUS-PSL (85.43%) and PRE-1000C (86.92%). These findings suggest potential utility for imaging-assisted ACO-related classification within this internal single-center evaluation. Further multi-center external validation and robustness analyses are warranted before conclusions regarding stability and generalizability can be made.

Keywords: deep learning, transfer learning, medical image segmentation, asthma-copd overlap

Introduction

Asthma typically has an earlier age of onset and is characterized by variable, intermittent symptoms. It generally responds well to inhaled corticosteroids and is frequently associated with allergic comorbidities. In contrast, chronic obstructive pulmonary disease (COPD) usually presents later in life with persistent symptoms, a slowly progressive course, and limited responsiveness to inhaled corticosteroids, and it is commonly linked to long-term tobacco exposure. Although asthma and COPD are distinct but prevalent respiratory diseases, they share certain risk factors and clinical manifestations, which can complicate differential diagnosis in real-world settings.

Deep learning has emerged as a powerful pattern-recognition technique inspired by neural networks and has been widely adopted in image analysis due to its capacity for hierarchical feature learning. In medical imaging, deep learning-particularly convolutional neural networks (CNNs)—has demonstrated strong potential for segmentation and classification tasks, motivating further investigation into its application for airway disease–related imaging analysis.

Building on this background, several studies have explored deep learning methods relevant to medical image understanding. Addagarla S K highlighted the utility of deep learning–based object detection for automated recognition tasks, demonstrating that model design and dataset scale can substantially affect performance in real-world applications.[1]

https://doi.org/10.2147/COPD.S578685
Received: 18 November 2025
Accepted: 9 March 2026
Published: 16 April 2026

Graphical Abstract

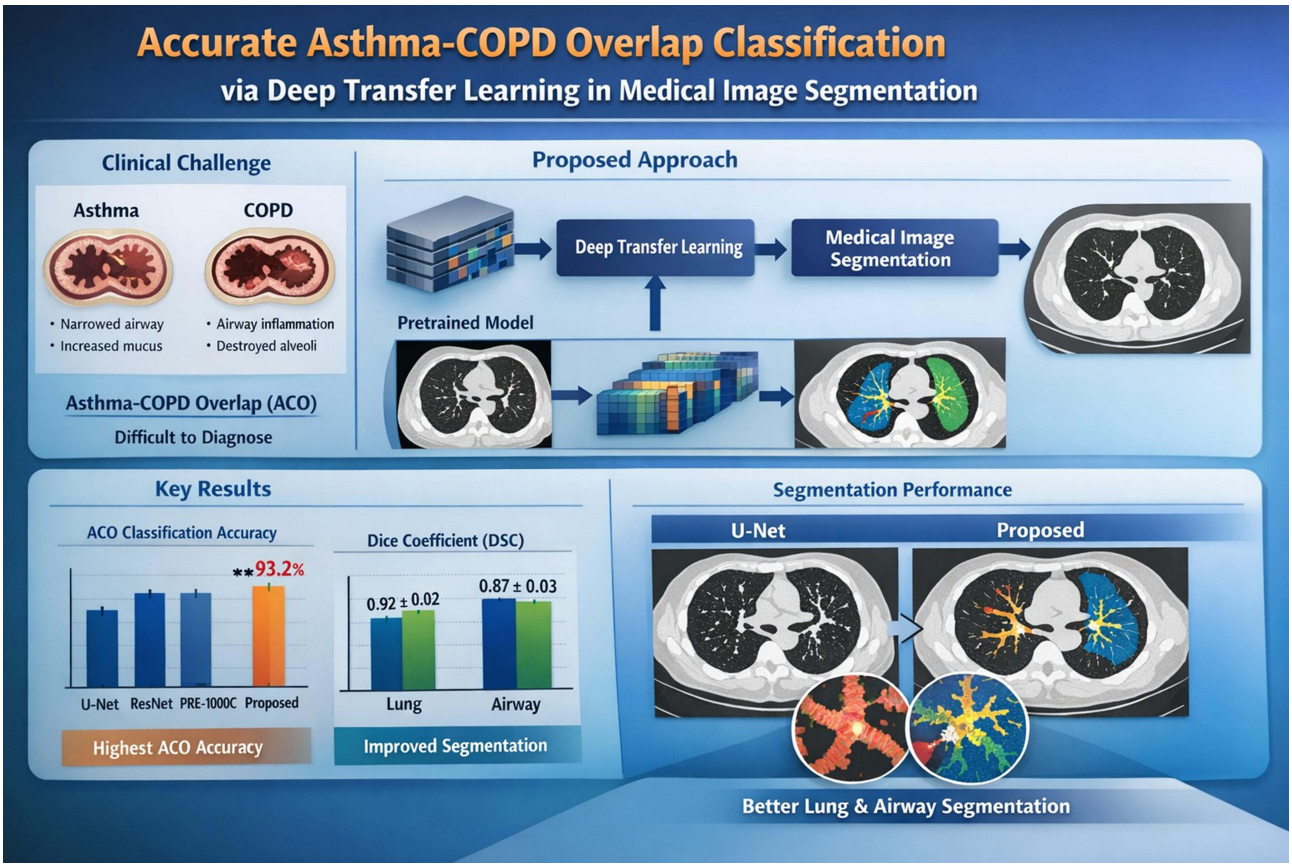

Wang emphasized that accurate medical image segmentation is essential for clinical decision-making and proposed an interactive segmentation approach that integrates CNN-based predictions with user feedback via geodesic distance transformation, achieving improved accuracy with reduced manual intervention compared with conventional interactive methods.[2] In addition, Yves L reviewed health-related quality-of-life (HRQL) assessment tools in COPD, underscoring the importance of symptom burden and functional status evaluation in comprehensive disease management.[3] Collectively, these studies suggest that combining advanced image analysis with clinical assessment may provide complementary insights into complex airway diseases.

In this study, we propose a chest CT image segmentation framework based on deep transfer learning for imaging-assisted classification of asthma, COPD, and asthma-COPD overlap (ACO). We first summarize advances in deep learning, CNN-based segmentation, and COPD-related clinical assessment to provide methodological and clinical context. We then describe the segmentation pipeline and transfer learning strategy and evaluate performance in a single-center cohort, using classification accuracy and Dice similarity coefficient as primary metrics. Clinical characteristics (including inflammatory biomarkers, lung function parameters, and ACT/CAT scores) were summarized to describe cohort profiles and support clinical interpretation; these variables were not predicted by the AI model. The proposed framework aims to extract complementary anatomical features from CT images that may assist phenotypic characterization of obstructive airway diseases. However, given the single-center design and limited sample size, the findings should be regarded as preliminary, and external validation is required to establish robustness and generalizability.

ACO is primarily defined by clinical symptoms, pulmonary function testing, bronchodilator responsiveness, and inflammatory biomarkers, and medical imaging alone is insufficient for definitive diagnosis. Nevertheless, computed

tomography (CT) can provide structural information regarding airway remodeling and lung parenchymal alterations, which may differ across asthma, COPD, and ACO phenotypes. Accordingly, in this work, medical image segmentation is applied as an adjunctive analytical approach rather than a standalone diagnostic method. By integrating deep transfer learning–based image analysis with established clinical and functional indicators, the proposed framework aims to extract complementary anatomical features that may support identification and stratification of obstructive airway diseases.

Overlapping Classification Method of Chronic Obstructive Pulmonary Disease and Asthma Lung Disease Based on Medical Image Segmentation Based on Deep Transfer Learning

Medical Image Segmentation

Medical images contain a large amount of information; however, clinicians typically focus on specific regions of interest (ROIs) relevant to diagnosis and treatment. Variations in imaging devices and acquisition protocols may introduce differing levels of noise and artifacts, which can degrade image quality and hinder accurate interpretation, thereby increasing the difficulty of clinical decision-making.[4,5] Consequently, medical image segmentation has attracted growing attention in both the medical and computer science communities as a key technique for extracting clinically meaningful structures from complex imaging data. Medical image segmentation aims to partition an image into multiple non-overlapping regions with distinct anatomical or pathological meanings, such that pixels (or voxels) within the same region share similar properties while different regions are clearly separated. Along with the continued development of classic segmentation approaches, a variety of new methods have emerged in recent years.[6] Given the diversity of segmentation techniques and the lack of a universally accepted taxonomy, this study introduces representative medical image segmentation methods from multiple perspectives to provide a structured overview.

Region-Based Segmentation Method

Region-based segmentation groups pixels (or voxels) with similar properties into coherent regions to separate target structures from the background. By leveraging local spatial characteristics, region-based methods typically produce spatially continuous segmentation results. However, because multiple candidate regions may satisfy similarity criteria, commonly used algorithms are prone to over-segmentation, particularly in the presence of noise, intensity inhomogeneity, or complex anatomical boundaries.[7]

Segmentation Method Based on K Nearest Neighbor

The k-nearest neighbors (KNN) algorithm is a supervised learning approach widely used in pattern recognition. In medical image segmentation, applying KNN typically requires manually annotated training data to provide representative labeled samples. For instance, in normal brain MR images, pixels corresponding to white matter, gray matter, and cerebrospinal fluid are often manually labeled based on expert knowledge to train and validate the classifier.[8]

First, select the K pixels with determined classifications that are closest to the pixel to be divided. If a certain medical image is divided into N categories, it is marked as $B_1, \ldots, B_N$. Among them, the number of the segmented pixels categories belonging to $B_1, \ldots, B_N$ of the K neighbors are $k_1, \ldots, k_N$ respectively, the category of the pixel to be segmented using the discriminant function. Among them, the discriminant function is defined as follows:

$$m(y) = (B_r | argmax(k_r))(r = 1, \ldots, N) \tag{1}$$

Among them, when we measure the similarity, we use Euclidean distance to measure, adding that the positions of the two pixels in the MR image space are yq_1 and yq_2 respectively. Then the Euclidean distance is defined as follows:

$$l(y_1, y_2) = \sqrt{(yq_1 - yq_2)^2} \tag{2}$$

Although KNN-based segmentation is conceptually simple and straightforward to implement, it often increases workload because it relies on manual labeling to obtain representative training samples. In addition, the choice of distance metrics and feature representations can substantially influence segmentation performance. Moreover, due to inherent intensity

inhomogeneity in MR images, gray-level–based classification approaches are susceptible to misclassification, particularly in regions with overlapping intensity distributions or bias-field artifacts.[9,10]

Clustering Segmentation Method Based on Fuzzy C-Means

Among fuzzy clustering techniques, fuzzy C-means (FCM) is one of the most widely used and successful methods. By minimizing an objective function, FCM computes the membership degree of each sample with respect to all cluster centers, thereby achieving unsupervised data partitioning. Each sample is associated with a set of membership values across clusters, and its cluster assignment is typically determined by the maximum membership principle.[11]

Use P(x) to mark an image, where x∈Ω, Ω represents the global image space. Assuming that the FCM algorithm divides the image P(x) into C categories, and record $k_n(n = 1, \ldots C)$ as the mean value of the nth category, then MR is the cluster center of the nth category at this time. We use the degree of membership to indicate the probability that a pixel y belongs to a certain category n, and the degree of membership is a value ranging from 0 to 1. We use $w_n(y)$ to indicate the degree of membership of the pixel y belonging to the category r, then we have:

$$\begin{cases} 0 \le w_n(y) \le 1 \\ \sum_{n=1}^{C} w_n(y) = 1 \end{cases} \tag{3}$$

The objective function of FCM can be expressed as follows:

$$f(k_n, w_n(y)) = \sum_{n=1}^{C} \sum_{y} w_n^k(y) ||P(y) - k_n||^2 \tag{4}$$

Based on the above constraints, the gradient descent method is used to update and solve the parameters k_n and $w_n(y)$. Then there are:

$$k_n = \frac{\sum_y w_n(y)/(y)}{\sum_y w_n(y)} \tag{5}$$

$$w_n(y) = \frac{1/||P(y) - k_n||^k}{\sum_{n=1}^{C} (1/||P(y) - k_n||^k)} \tag{6}$$

Using the above formula to update the parameters k_n and $w_n(y)$, it can be seen that the change of the objective function is very small and the iteration stops. If we directly use the FCM algorithm on medical images, such as MR images, this clustering method based on image gray will be greatly affected due to the unevenness of the gray level of the medical image itself.[12]

Chronic Obstructive Pulmonary Disease and Asthmatic Lung Disease

Asthma and chronic obstructive pulmonary disease (COPD) are two common chronic airway diseases that are often considered in differential diagnosis in clinical practice. Figure 1 illustrates schematic bronchial changes associated with asthma and COPD. In some patients, however, an immediate and definitive distinction cannot be made, and clinical management may therefore incorporate elements of both treatment strategies with longitudinal assessment during follow-up.[13] Inflammatory profiles may also overlap. For example, eosinophilic airway inflammation can be observed in a subset of COPD patients, particularly during acute exacerbations, whereas neutrophilic inflammation may become more prominent in patients with more severe asthma. With increasingly detailed investigations into the pathophysiology of asthma and COPD, the concept of overlapping phenotypes has gained attention, prompting growing interest in asthma–COPD overlap (ACO).[14] Given its mixed clinical features and potential implications for disease control, the management of ACO has become a topic of considerable concern among clinicians.

In current clinical practice, management of asthma–COPD overlap (ACO) is largely extrapolated from treatment strategies for asthma and COPD, and dedicated guideline recommendations remain under development. For asthma control, inhaled corticosteroid/long-acting β2-agonist (ICS/LABA) combinations such as budesonide-formoterol are

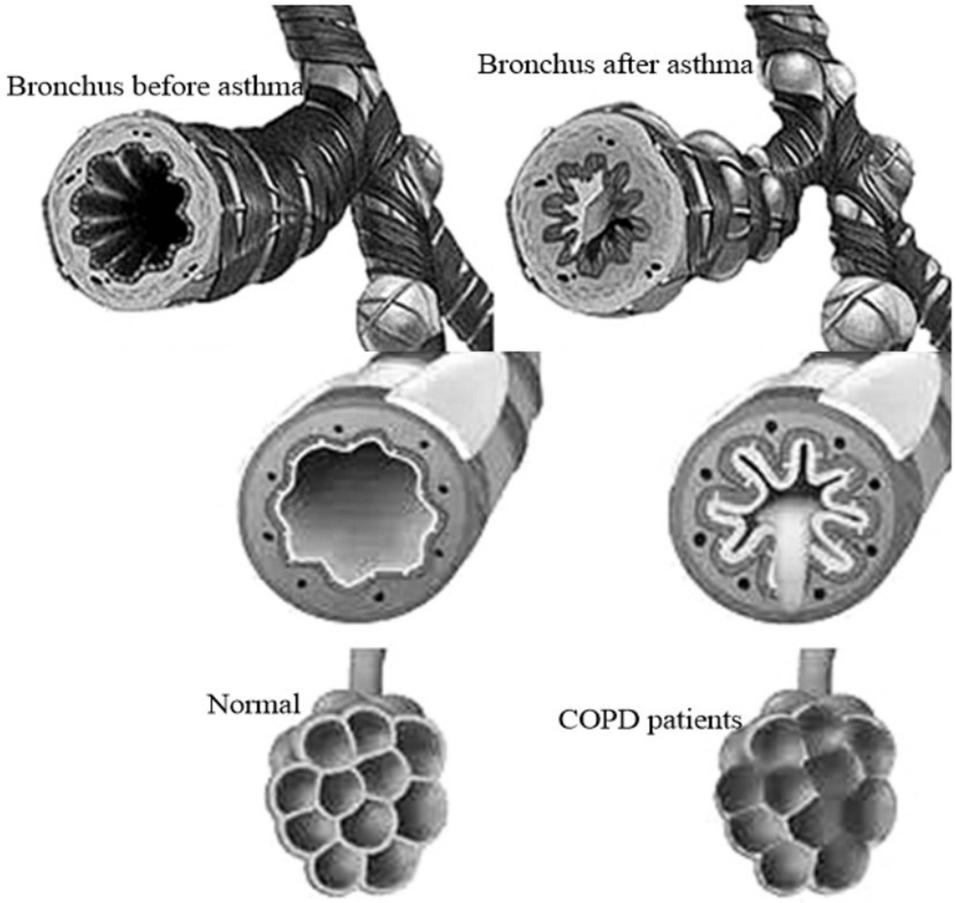

Figure 1 Schematic illustration of bronchial structural differences between asthma and COPD. This figure is provided for conceptual background only and does not represent quantitative measurements or study-derived imaging results.

commonly prescribed. In patients with more prominent COPD features or greater airflow limitation, add-on long-acting muscarinic antagonists (LAMAs) such as tiotropium bromide may be considered. Compared with ACO, non-ACO COPD phenotypes may demonstrate more consistent treatment responses to corticosteroid-containing regimens in selected clinical contexts.[15,16] However, how therapeutic responses differ among patients with ACO, asthma, and COPD remains incompletely understood. Tiotropium bromide is a widely used LAMA for chronic airway diseases. Owing to its prolonged bronchodilatory effect and relatively low systemic absorption, it is generally associated with sustained efficacy and a favorable safety profile. Although evidence supporting tiotropium in asthma and COPD is relatively robust, earlier studies frequently excluded ACO because of limited and evolving definitions. With increasing research attention and iterative updates of disease concepts and guidance, ACO is being more clearly characterized, which facilitates more standardized diagnosis, management, and clinical investigation. Nevertheless, optimizing treatment strategies for ACO-including severity-based medication selection, dose adjustment, treatment duration, and criteria for step-down or discontinuation-requires larger-scale, well-designed clinical studies.[17]

Transfer Learning

Transfer learning aims to leverage knowledge learned from a task in a source domain and apply it to a related task in a target domain to improve performance on a new problem. This paradigm is particularly useful when the target domain lacks sufficient labeled data or computational resources for effective model training. In practice, transfer learning often initializes a target model with parameters pretrained on a large source dataset and then fine-tunes the model on the target dataset, thereby accelerating convergence and improving generalization under limited data conditions.[18,19] In

conventional machine learning, classification models are typically trained using sufficiently large labeled datasets, and it is generally assumed that the training and test data follow the same or similar distribution. These requirements impose substantial costs for data collection and annotation, and obtaining large-scale, high-quality labeled medical data is often challenging in real-world settings. Moreover, distribution shifts across scanners, protocols, or institutions may further limit the applicability of models trained in a single dataset. Unlike traditional approaches that rely primarily on learning from the target domain, transfer learning explicitly exploits representations learned in the source domain to support recognition tasks in the target domain, thereby mitigating data scarcity and domain shift to some extent.[20] Figure 2 illustrates the general workflow of transfer learning.

In transfer learning, transfer component analysis (TCA) is used to reduce the dimensionality of the data that needs to be transferred, so as to remove redundant information. TCA is a feature-based transfer learning method, which needs to solve the problem of regional adaptation.[21]

Assuming that there is a feature map R, the edge distribution of the source domain and target domain data after the mapping will be close, namely:

$$T(R(Y_k)) \approx T(R(Y_L)) \tag{7}$$

The corresponding conditional distribution is:

$$T(Z_K|R(Y_k)) \approx T(Z_L|R(Y_L)) \tag{8}$$

In this way, the regional adaptation problem is solved. Since the essence of transfer learning is to minimize the distance between the source domain and the target domain, R can be solved by solving the minimum distance between the source domain and the target domain. TCA uses the maximum mean difference to solve the minimum distance, namely:

$$dist\left(Y'_{src}, Y'_{tar}\right) = \left|\left|\frac{1}{i_1}\sum_{n=1}^{i_1} R(y_{src_n}) - \frac{1}{i_2}\sum_{n=1}^{i_2} R(y_{tar_n})\right|\right|^2 \tag{9}$$

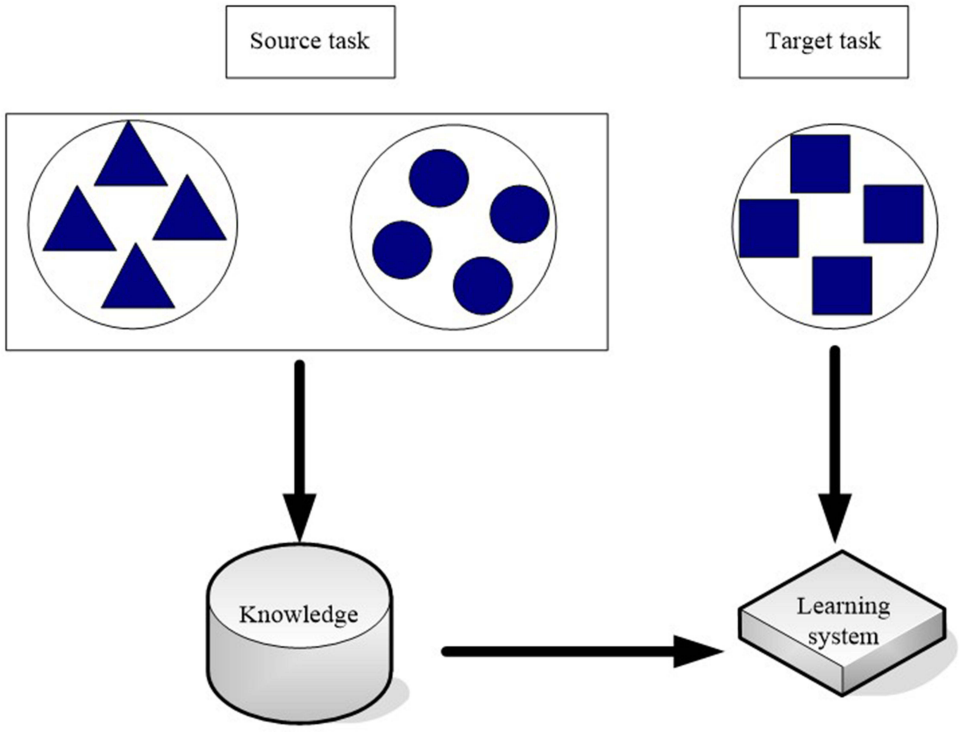

Figure 2 Schematic diagram of the transfer learning framework. A pretrained backbone network is adapted from a source domain and fine-tuned on the target medical imaging dataset to support task-specific segmentation.

The above formula will have a quadratic product term after the square expansion. The kernel function is used to find a more difficult mapping in the form of a kernel function, so TCA introduces the kernel matrix M:

$$M = \begin{bmatrix} M_{src,src} & M_{src,tar} \\ M_{tar,tar} & M_{tar,tar} \end{bmatrix} \tag{10}$$

The corresponding coefficient matrix U is:

$$U_{no} = \begin{cases} \frac{1}{i_1^2} & y_n, y_o \in Y_{src} \\ \frac{1}{i_2^2} & y_n, y_o \in Y_{tar} \\ -\frac{1}{i_1 i_2} & otherwise \end{cases} \tag{11}$$

Then the objective function can be written as:

$$trace(MU) - \eta trace(M) \tag{12}$$

Among them, trace is the trace of the matrix, which contains a semi-definite programming (SDP) problem, which is very time-consuming to solve, so the kernel matrix $\tilde{M}$ is reduced in dimensionality,[22] namely:

$$\tilde{M} = \left(MM^{-1/2}\tilde{Z}\right)\left(\tilde{Z}^{\tilde{L}}M^{-1/2}M\right) = \left(MZZ^{L}M\right) \tag{13}$$

The Z in the above formula is a matrix with a lower dimension than M, so the SDP problem is solved. The final optimization goal of TCA is:

$$\begin{aligned} &\min_{Z} tr\left(Z^{L}MUZ\right) + \lambda tr\left(Z^{L}Z\right) \\ &s.t. \quad Z^{L}MGZ = N_q \end{aligned} \tag{14}$$

Where m is the eigenvalue and G is the central matrix.

$$G = N_{i_1+i_2} - 1/(i_1 + i_2)NN^{L} \quad N \in Q^{i_1+i_2} \tag{15}$$

TCA can completely transform the problem into a mathematical problem when extracting the transfer components, and use pure mathematical tools to solve it. Another advantage is that the optimization of the matrix is done in place, so its implementation is very simple and does not have too many restrictions. But the disadvantage is that the decomposition of large matrices is not completely solved, which results in the calculation is still very time-consuming.[23]

Deep Learning

Deep neural networks have achieved strong performance across a wide range of machine learning tasks, including computer vision, speech processing, and affective computing. Their success is largely attributed to the ability of deep architectures to learn hierarchical, nonlinear feature representations directly from input data. Common deep learning models include autoencoders, convolutional neural networks (CNNs), restricted Boltzmann machines (RBMs), and recurrent neural networks (RNNs), among others.

Autoencoders are unsupervised deep learning models designed to learn efficient representations of input data, typically by reconstructing the input at the output layer. Their architecture consists of two parts: an encoder, which maps the input to a lower-dimensional latent representation, and a decoder, which reconstructs the original input from this latent code. When the latent space has fewer dimensions (or fewer neurons) than the input, the model learns a compressed representation, analogous to dimensionality reduction or data compression. Many modern generative models build on the autoencoder paradigm, such as variational autoencoders and related extensions, which have attracted substantial research attention in recent years.[24]

Convolutional neural networks (CNNs) offer two key advantages: local connectivity and weight sharing. Local connectivity is well suited for two-dimensional and higher-dimensional image data because convolutional filters operate on spatially localized regions (local receptive fields) as they slide across the input. This enables CNNs to capture spatially structured patterns while preserving positional relationships among features. In addition, convolutional operations

provide a degree of translation equivariance, which supports robust feature extraction under spatial shifts. Weight sharing further improves efficiency by applying the same filter parameters across different spatial locations. Multiple convolutional filters are learned, and each filter produces a corresponding feature map from the input image. By reusing the same filter weights across the entire image, CNNs substantially reduce the number of learnable parameters compared with fully connected architectures, thereby lowering computational cost and mitigating overfitting risk.[25] Figure 3 illustrates the basic architecture of a CNN.

Implementation Details of the Deep Transfer Learning Model

All experiments were implemented using the PyTorch deep learning framework (version 1.12) on a workstation equipped with an NVIDIA RTX 3090 GPU (24 GB memory). The operating system was Ubuntu 20.04 with Python 3.8, CUDA 11.6, and cuDNN 8.4. All images used in this study were chest computed tomography (CT) scans. CT images were preprocessed by applying a Hounsfield unit (HU) window of −1000 to 400, followed by min–max normalization. Images were resampled to an in-plane resolution of 1.0×1.0 mm and resized to 512×512 pixels. Axial CT slices were used as model inputs. The segmentation network adopted an encoder–decoder architecture based on a U-Net–like design. A ResNet-50 backbone pretrained on ImageNet was employed as the encoder to initialize model weights via transfer learning. The decoder consisted of upsampling layers with skip connections to preserve spatial details. The network output included three classes: background, lung parenchyma, and airway-related structures. Transfer learning was applied by initializing the encoder with pretrained ImageNet weights, while all network layers were fine-tuned during training. Model optimization was performed using the Adam optimizer with an initial learning rate of 1×10^{-4} and a weight decay of 1×10^{-5}. The batch size was set to 8, and the maximum number of training epochs was 100. Early stopping was applied if no improvement in validation loss was observed for 15 consecutive epochs. A ReduceLROnPlateau scheduler was used to adaptively decrease the learning rate. The loss function consisted of a weighted combination of Dice loss and cross-entropy loss, with increased weighting applied to airway structures to address class imbalance. Data augmentation strategies included random rotations (±10°), horizontal and vertical flipping, scaling (0.9–1.1), and Gaussian noise injection (σ= 0.01). The dataset comprised 200 patients and was split at the patient level into training (70%), validation (15%), and test (15%) sets using stratified random sampling to avoid data leakage. Segmentation performance was

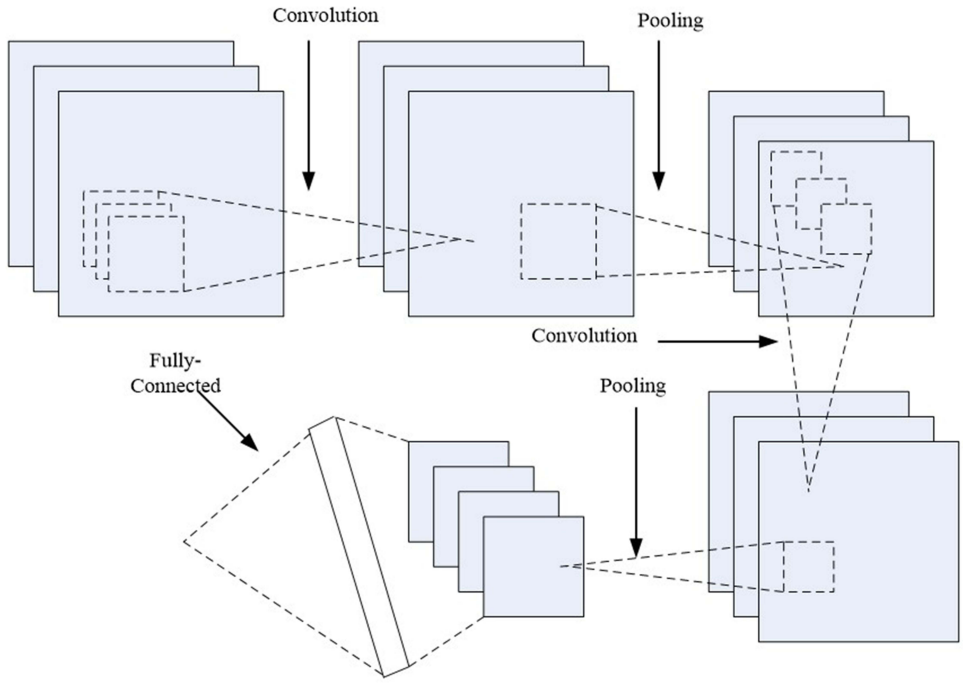

Figure 3 Basic architecture of a convolutional neural network (CNN). This diagram illustrates the general structure of CNNs and is included for methodological background.

evaluated on the independent test set using the Dice similarity coefficient (DSC). For model comparison, paired statistical tests were conducted, and a two-sided p value < 0.05 was considered statistically significant.

Ground-Truth Annotation and Dice Coefficient Calculation

All chest CT images were manually annotated to generate reference segmentation masks. Two board-certified radiologists with 6 and 10 years of experience in thoracic imaging independently delineated the target anatomical structures using standardized labeling guidelines and dedicated medical image annotation software. Discrepancies between annotations were resolved through consensus discussion, and unresolved cases were adjudicated by a senior radiologist. For quality control, a random sample of 20% of cases was re-reviewed to ensure labeling consistency. Segmentation performance was quantitatively evaluated using the Dice similarity coefficient (DSC), defined as $DSC = 2|P \cap G|/(|P| + |G|)$, where P denotes the predicted mask and G denotes the reference mask. DSC was calculated on the independent test set for each anatomical structure on a per-subject basis.

Overlap Classification Experiment of Chronic Obstructive Pulmonary Disease and Asthma Lung Disease Based on Medical Image Segmentation Based on Deep Transfer Learning

Research Objects

We selected 200 patients who were admitted to the Department of Respiratory Medicine of a tertiary hospital from January 2020 to May 2021. Among them, 142 were male patients and 58 were female patients. The study was conducted with a prospective method.

Exclusion criteria: 1) acute COPD, acute asthma attack; 2) the patient had previously undergone lung resection; 3) combined with a history of severe pulmonary fibrosis; 4) combined with a history of tuberculosis; 5) combined with a history of lung cancer; 6) combined with pulmonary embolism Medical history; 7) Use of systemic glucocorticoids due to other underlying diseases; 8) Failure to communicate well with clinicians.

Inclusion criteria for the control group: ①Past physical fitness, no history of serious heart and cerebrovascular diseases and chronic respiratory diseases. ②There was no history of upper respiratory tract infection in the past 2 weeks. ③Patients have the ability to cooperate with clinicians to perform lung function tests.

Inclusion criteria for the COPD group: (1) Aged over 40 years old, patients with cough, sputum expectoration, and difficulty breathing after activities, lung function tests revealed persistent airflow limitation, that is, after the use of albuterol 400ug or other bronchodilators, The ratio of the forced expiratory volume in the first second to the forced expiratory volume should be less than 0.7. (2) The patient needs to be hospitalized for treatment due to respiratory system related symptoms such as cough, sputum expectoration, or dyspnea.

Inclusion criteria for the ACO group: Patients diagnosed with chronic obstructive pulmonary disease based on smoking history, symptoms, age, and lung function test results. If the patient currently meets the diagnosis of asthma, the diagnosis of ACO can also be established immediately. If the diagnosis of asthma is not currently met, At least one of the following criteria should be met: (1) The bronchodilation test is strongly positive (after inhaling the bronchodilator, the FEV1 improvement rate is ≥15% and the absolute value is ≥400mL). (2) Blood eosinophils ≥300c/μL. All medical images analyzed in this study were chest computed tomography (CT) images, acquired as part of routine clinical assessment.

Observation Indicators

FEV1, FVC, one-second rate (FEV1/FVC), PEF, MMEF, MEF75, MEF50, MEF25, RV, TLC, residual/total ratio (RV/TLC), carbon monoxide dispersion (DLco).

Instruments

The main equipment used in this study includes: pulmonary function meter, COPD patient self-assessment test questionnaire, asthma control test, enzyme label analyzer, automatic blood analyzer, blood gas analyzer, ultra-low temperature storage box, etc.

The assessment of the asthma control test consists of 5 parts: the time is the same in the past 4 weeks, the degree of interference of the patients with asthma symptoms on daily activities, the frequency of dyspnea caused by the patient's asthma symptoms, and the degree of impact of asthma during night rest. The frequency of emergency medication use, and my own evaluation of the degree of control of my own asthma. A full score indicates complete control of asthma symptoms; a lower score indicates poorer asthma control.

The COPD patient self-assessment test questionnaire score is divided into 8 questions, with a total score of 40 points. The more severe the symptoms, the higher the score. When the score exceeds 10 points, the comprehensive evaluation of COPD indicates severe symptoms. Including the typical symptoms of COPD, such as cough, sputum, chest tightness, etc. COPD causes the patient's impact on climbing or stairs, indoor activities, going out, sleep and energy.

Experimental Method

According to the Spanish Asthma-COPD Overlapping Consensus established in 2017, the diagnostic criteria are divided into ACO group and COPD group. Taking acute exacerbation and survival status as the main indicators for observing prognosis, the collected clinical data was analyzed statistically using SPSS and STATA software including *t*-test, rank-sum test, chi-square test and Z-test.

Model Comparison

To provide a more comprehensive benchmark evaluation, widely used medical image segmentation frameworks, including U-Net and its variants, were incorporated as additional comparative models. These models were implemented using standard configurations reported in the literature and trained on the same dataset under identical experimental conditions to ensure fair comparison.

Chronic Obstructive Pulmonary Disease and Asthma Lung Disease Based on Deep Transfer Learning Medical Image Segmentation Overlapping Classification Analysis

All figures are presented with quantitative annotations, including sample sizes, variability measures, and statistical summaries, to facilitate objective interpretation of model performance. A total of 200 subjects were included and categorized into normal, COPD, asthma, and asthma-COPD overlap (ACO) groups. Clinical characteristics (lung function parameters, inflammatory biomarkers, and ACT/CAT scores) were summarized to describe cohort profiles and support clinical phenotyping. Importantly, these variables were not predicted by the AI model; rather, they were used to provide clinical context and to aid interpretation of the imaging segmentation–based classification results. The following sections report segmentation performance (Dice coefficient), classification performance, and the clinically contextualized interpretation of the findings.

Table 1 Comparison of Classification Accuracy of Each Method

Model	Normal	COPD	Asthma	ACO
Deep transfer learning	95.16	94.29	94.12	93.21
NUS-PSL	91.24	90.24	91.03	85.43
PRE-1000C	90.14	89.04	90.21	86.92
REA-C1000	92.24	88.31	89.42	89.32
CNN	92.57	91.23	92.14	91.45

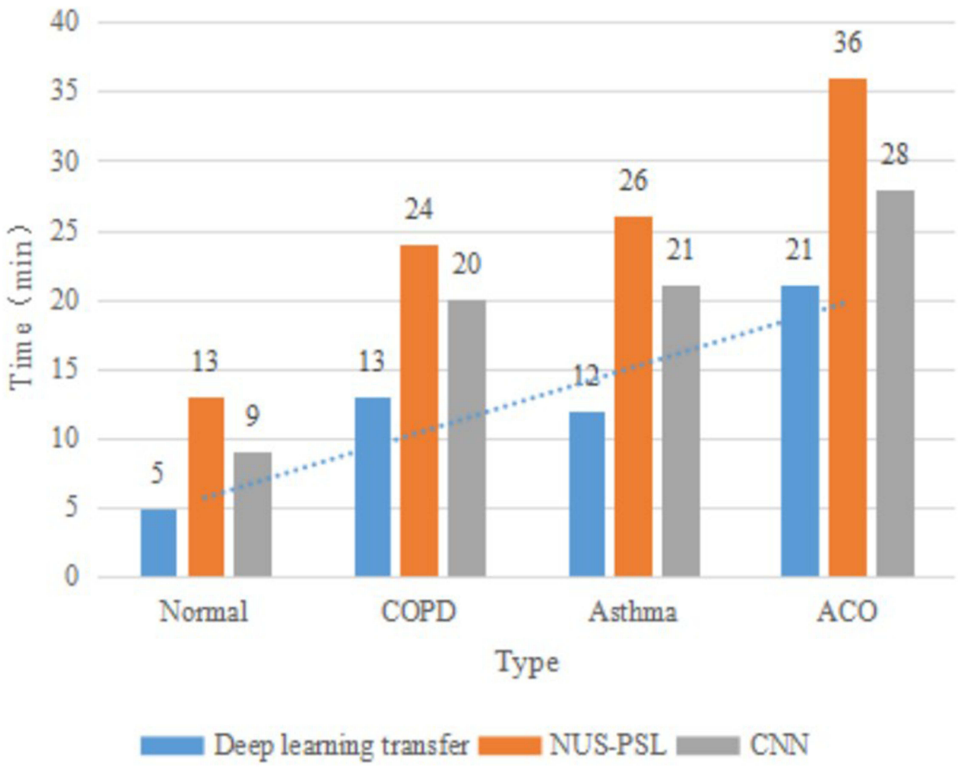

Figure 4 Comparison of segmentation time across different models and disease categories. Bars represent mean segmentation time, and error bars indicate standard deviation across repeated runs. n = 200 subjects.

Recognition Accuracy

By collecting the medical images of the 200 patients, using the deep transfer learning algorithm and the four algorithms of NUS-PSL, CNN, PRE-1000C and REA-C1000 to identify and classify the collected 200 medical images The accuracy rate is shown in Table 1.

Figure 4 shows the time taken by the three algorithms to segment medical images of patients with normal conditions, COPD, asthma, and ACO. Obviously, the three algorithms have the fastest recognition speed for normal conditions. This is because there are no obvious lesions in medical images under normal conditions. Deep transfer learning only takes five minutes, while the NUS-PSL algorithm takes 13 minutes and the CNN algorithm takes 9 minutes. However, when recognizing medical images of ACO patients, the speed of the three is significantly reduced. It can be seen that the recognition of ACO is more difficult, but deep transfer learning still maintains a speed better than the other two algorithms.

Dice Coefficient Analysis

Figure 5 shows the change of the Dice coefficient during the training process. The test results in this article compare the Dice coefficients of lung, pharynx, larynx, and bronchus in ACO patients, which is a commonly used image segmentation evaluation method. It can be seen from Figure 5 that as the time period increases, the Dice coefficient of all organs has an upward trend, and the Dice coefficient of the lungs has always been at a relatively high level. It can be seen that the method used in this paper can segment the image of the lung Good, but the segmentation effect of the bronchus and throat needs to be strengthened, and the longer the period, the higher the Dice coefficient, which shows that the test time of these medical images is relatively long. This is because the pixels at the center point are processed. The segmentation method contains millions of parameters, and the deep transfer learning used in this article involves a convolutional neural network, which makes it take a long time for each medical image to achieve segmentation analysis.

https://doi.org/10.2147/COPD.S578685

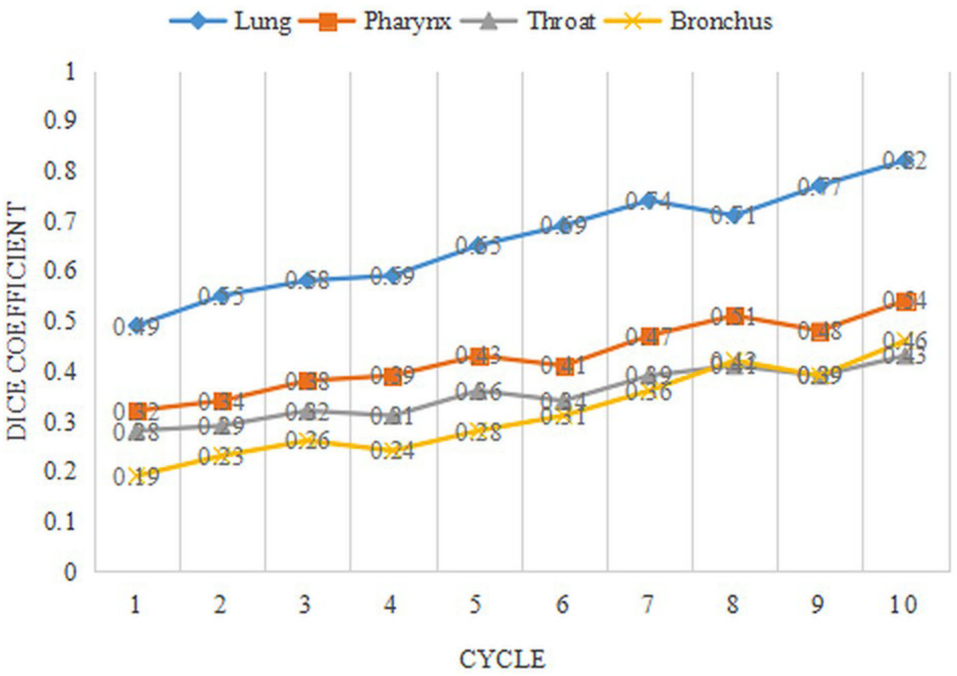

Figure 5 Dice coefficient curves during model training. Dice similarity coefficients were calculated between predicted masks and expert-annotated reference masks on the independent test set. Curves represent lung parenchyma, bronchus, pharynx, and larynx structures, demonstrating stable convergence across training epochs.

General Information Situation

The general characteristics of patients in the COPD and ACO groups are summarized in Table 2. Compared with the COPD group, patients in the ACO group had a significantly higher BMI (25.78±4.21 vs. 24.89±3.27, P=0.001), whereas the mean age was slightly lower (74.23±9.12 vs. 75.21±8.98, P=0.003). Smoking duration and the number of cigarettes smoked per day were both significantly lower in the ACO group than in the COPD group (P=0.001 for both). No significant differences were observed between the two groups with respect to sex distribution or length of hospital stay (both P>0.05), as shown in Table 2.

Inflammation Indicators Analysis

The comparison of inflammatory indicators between the COPD and ACO groups is presented in Table 3. Blood eosinophil levels were markedly higher in the ACO group than in the COPD group (0.29±0.28 vs. 0.07±0.08, P<0.001), and serum IgE levels also tended to be higher in the ACO group, although this difference did not reach statistical significance (P=0.139). In contrast, leukocyte count, neutrophil count, erythrocyte sedimentation rate, C-reactive protein, and procalcitonin levels

Table 2 Comparison of General Indicators of COPD Patients and ACO Patients

		COPD Group	ACO Group	x^2/t	P
BMI		24.89±3.27	25.78±4.21	−3.124	0.001
Age		75.21±8.98	74.23±9.12	2.753	0.003
Gender	Male	66	62	5.321	0.587
	Female	34	38		
Smoking days		29.67±14.27	27.43±15.89	−2.978	0.001
Number of smoking (pieces per day)		9.67±5.78	8.68±9.34	−2.384	0.001
Hospital stay		9.23±3.48	8.92±3.13	1.392	0.178

Table 3 Comparison of Inflammatory Indexes Between COPD Patients and ACO Patients

	COPD Group	ACO Group	x^2/t	P
Leukocyte	10.78±3.98	9.89±3.67	2.314	0.012
Neutrophils	8.23±3.92	6.34±2.89	3.423	<0.001
IgE	99.46±116.35	121.87±146.53	−1.456	0.139
Blood eosinophils	0.07±0.08	0.29±0.28	−9.039	<0.001
Erythrocyte sedimentation rate	42.56±29.67	32.57±22.75	2.867	0.006
C reactive protein	49.18±59.82	28.94±44.89	3.283	0.003
Procalcitonin	0.59±2.34	0.28±0.21	−1.969	0.046

Table 4 Irrational Medication Performance

Types of Unreasonable Drug Use	Number of Cases	Percentage
Failure to adjust the drug treatment plan in time according to changes in the condition, and change the drug at will.	15	7.5%
Inappropriate combined use of bronchodilators and glucocorticoids	12	6%
Antibiotic abuse	11	5.5%
Single mode of administration	8	4%
Unreasonable timing of medication	7	3.5%

were all lower in the ACO group than in the COPD group. Among these indicators, leukocyte count (P=0.012), neutrophil count (P<0.001), erythrocyte sedimentation rate (P=0.006), C-reactive protein (P=0.003), and procalcitonin (P=0.046) showed statistically significant between-group differences, as shown in Table 3.

Performance of Irrational Drug Use

The patterns of irrational medication use among patients are summarized in Table 4. The most common problem was failure to adjust the treatment regimen in a timely manner according to changes in the patient's condition, accounting for 7.5% of cases. This was followed by inappropriate combined use of bronchodilators and glucocorticoids (6.0%), antibiotic abuse (5.5%), single mode of administration (4.0%), and unreasonable timing of medication (3.5%). These findings indicate that although the overall proportion of irrational medication use was relatively low, medication management in some patients still requires improvement, as shown in Table 4.

Comparison of Lung Function Indicators

As shown in Figure 6, the FEV1, FVC, FEV1/FVC indicators indicate airflow limitation. In this article, the asthma group, COPD group, and ACO group patients all decreased compared with the control, indicating that asthma, COPD and ACO patients all have airflow limitation Compared with asthma patients alone, the ACO group had more severe airway obstruction (P<0.05). This can be explained by the fact that smoking can significantly accelerate the decline of lung function in subjects with or without asthma, and ACO patients have more smokers than asthma patients alone. There was no significant difference between patients in the ACO group and COPD alone (P>0.05). The lung function decline of COPD patients alone is more significant than that of ACO patients. From the figure, it can be seen that FEV1 of ACO patients is 45%, and FEV1 of COPD patients is 41%. It can be seen that the lung function of ACO patients is

 https://doi.org/10.2147/COPD.S578685

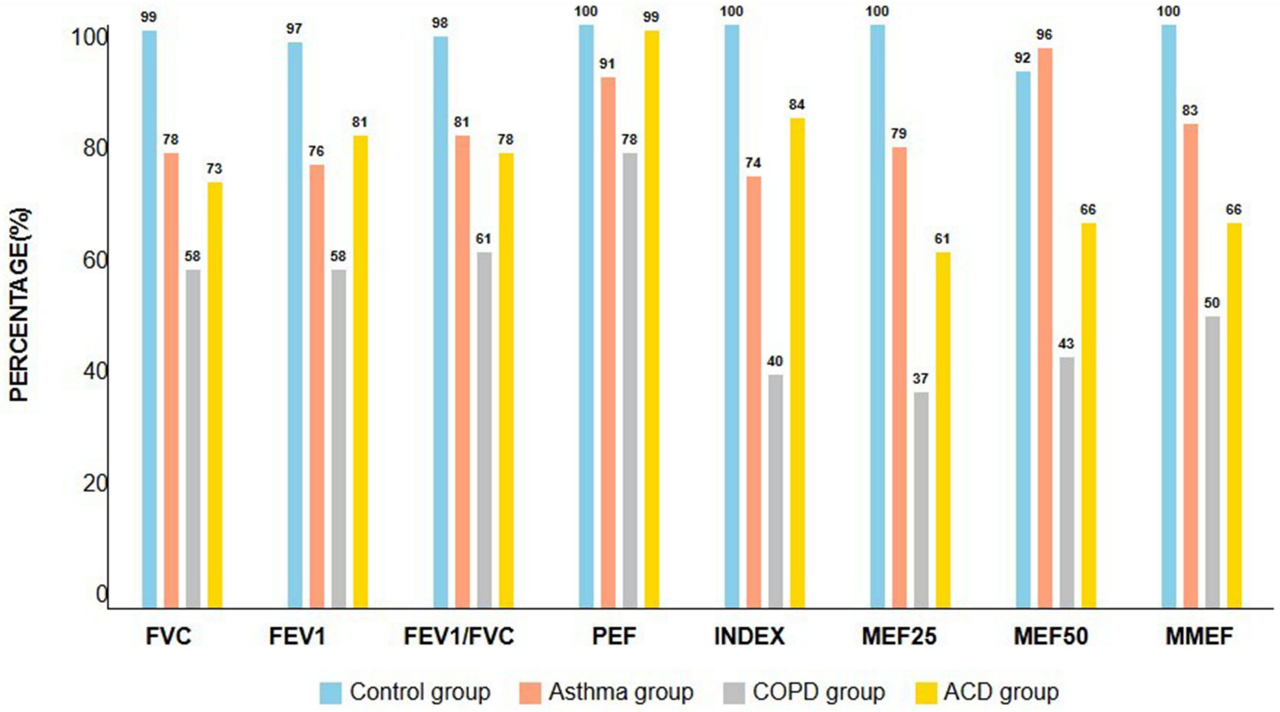

Figure 6 Comparison of lung function in each group.

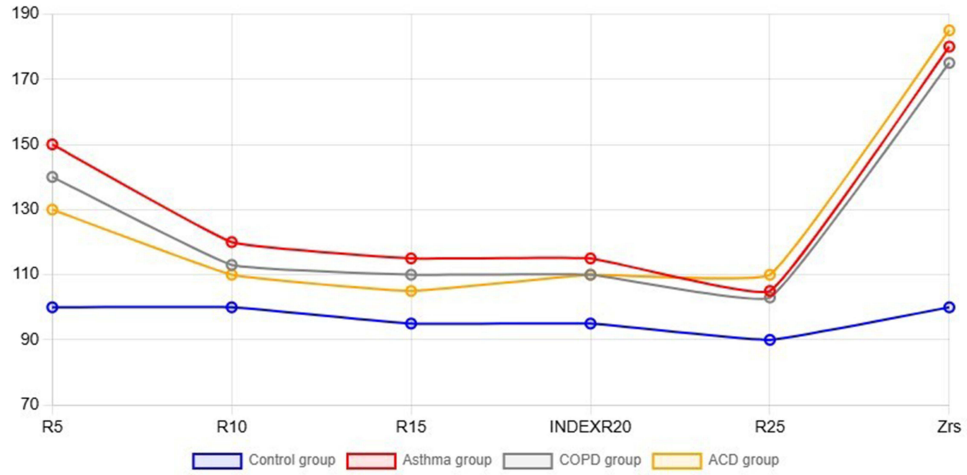

Figure 7 Comparison of airway resistance in each group.

significantly better than that of COPD patients. Two indicators, MEF50 and MEF25, can be used to indicate the degree of small airway obstruction. In this article, patients in the asthma group, COPD group, and ACO group are all lower than the control, indicating that patients with asthma, COPD and ACO all have small airway dysfunction. Patients in the ACO group Compared with patients with asthma alone, small airway obstruction was more serious ($P<0.05$), and there was no significant difference compared with patients with COPD alone ($P>0.05$).

Figure 7 is a comparison chart of the airway resistance of each group. The total respiratory impedance is represented by Zrs, the total airway resistance is represented by R5, R5-R25 is the respiratory resistance at different hertz, and R20 is the central airway resistance. Compared with the control group, the Zrs and R5-R25 of the COPD group and asthma patients increased, which exceeded those of the control group.

Table 5 Comparison of Patients' ACT Score and CAT Score Before and After Treatment

Group	Cases	Time	ACT Score	CAT Score
Asthma	54	Before treatment	16.8±2.9	—
		After treatment	23.7±2.5	—
COPD	46	Before treatment	—	27.5±3.2
		After treatment	—	23.1±2.6
ACO	43	Before treatment	16.8±2.3	23.2±2.9
		After treatment	18.9±3.0	21.3±2.3

ACT and CAT Score Analysis

Changes in ACT and CAT scores before and after treatment are shown in Table 5. All three groups showed improvement after treatment. In the asthma group, the ACT score increased from 16.8±2.9 before treatment to 23.7±2.5 after treatment, indicating a relatively marked improvement in symptom control. In the COPD group, the CAT score decreased from 27.5±3.2 to 23.1±2.6 after treatment. In the ACO group, the ACT score increased from 16.8±2.3 to 18.9±3.0, whereas the CAT score decreased from 23.2±2.9 to 21.3±2.3. Overall, the improvement in the ACO group was less pronounced than that in the asthma group, which may be related to the coexistence of partially reversible and persistent airflow limitation in ACO, as shown in Table 5.

Classification Performance Comparison

A total of 200 subjects were included and classified into normal, COPD, asthma, and asthma–COPD overlap (ACO) groups. The classification performance of the proposed deep transfer learning–based method was compared with NUS-PSL, PRE-1000C, REA-C1000, and conventional CNN models. The proposed method achieved consistently high accuracy across all disease categories. In particular, the ACO classification accuracy of the proposed method reached 93.21%, which was higher than that of NUS-PSL (85.43%), PRE-1000C (86.92%), REA-C1000 (89.32%), and CNN (91.45%). These results indicate that the proposed approach demonstrates improved discrimination ability for complex

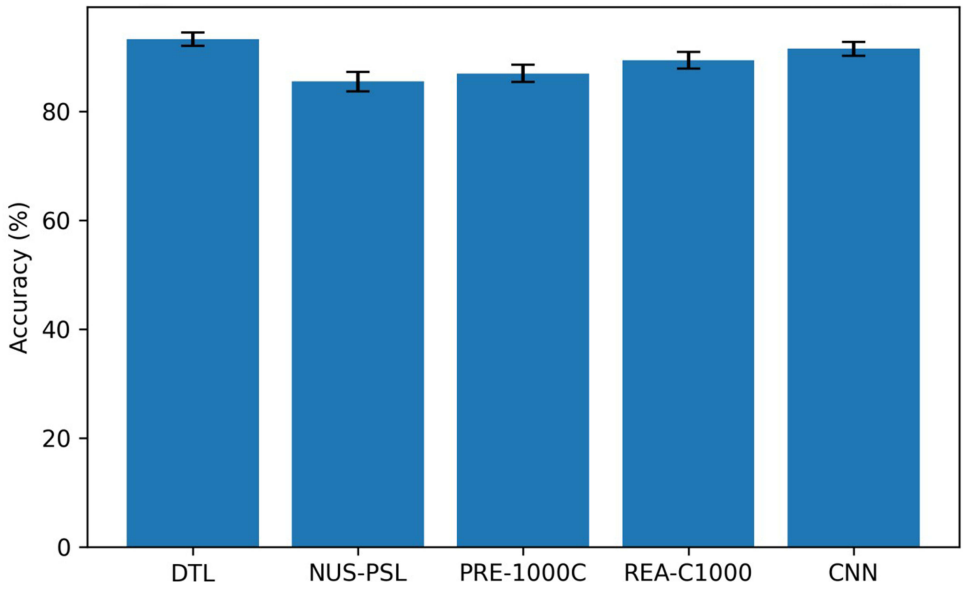

Figure 8 Presents a comparison of ACO classification accuracy across different models. Error bars represent 95% confidence intervals (CI) estimated based on the binomial distribution of classification outcomes.

https://doi.org/10.2147/COPD.S578685

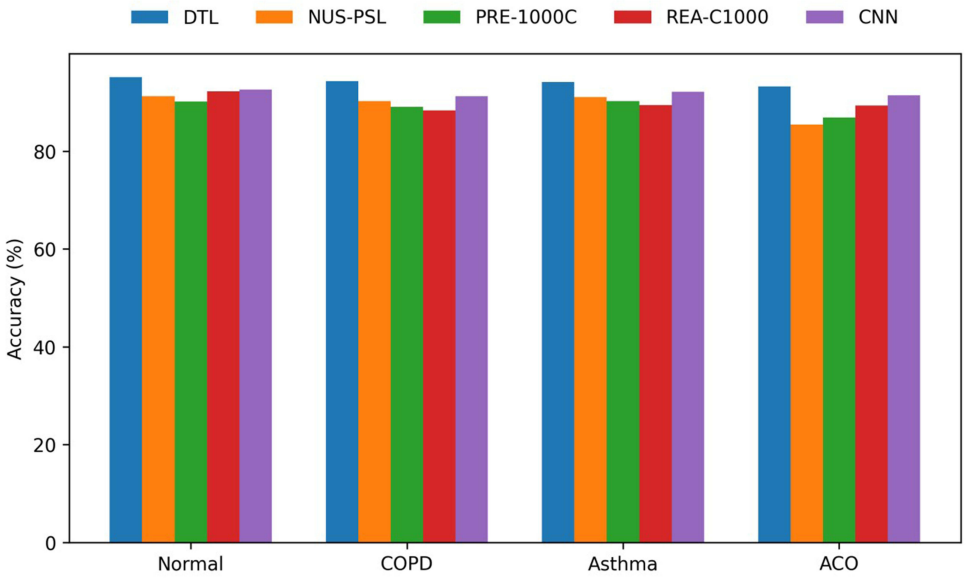

Figure 9 Further illustrates classification accuracy across all disease categories. The proposed method consistently outperformed comparative models in normal, COPD, asthma, and ACO groups.

overlapping airway disease phenotypes. The comparison of ACO classification accuracy across different models is illustrated in Figure 8, whereas the classification performance across all disease categories is presented in Figure 9.

Statistical Significance Analysis

To further assess whether the observed performance differences were statistically meaningful, statistical analyses were conducted on ACO classification accuracy. Pairwise comparisons between the proposed deep transfer learning-based method and comparative models were performed using paired statistical tests on the independent test set. The proposed method demonstrated statistically significant improvements in classification accuracy compared with the NUS-PSL and PRE-1000C models (two-sided $P< 0.05$). These results suggest that the observed performance differences are unlikely to be attributable solely to random variation within the evaluated dataset. However, given that the analysis was based on a single-center cohort without external validation, the statistical findings should be interpreted with caution, and further confirmation in independent datasets is warranted.

Dice Coefficient Analysis

The Dice coefficient was used to quantitatively evaluate segmentation performance. Dice values were calculated between automated segmentation results and expert-annotated reference masks. As shown in Figure 10, Dice coefficients for all models increased with training progression, demonstrating stable convergence. The proposed method consistently achieved higher Dice coefficients than comparative models across most anatomical structures. Lung parenchyma segmentation yielded higher Dice values than airway-related structures, reflecting the increased complexity of airway boundary delineation. Detailed quantitative Dice similarity coefficient results for different anatomical structures are presented in Table 6.

Visualization of Segmentation Results

Representative segmentation results are shown in Figure 11. Compared with other models, the proposed method produced more continuous and accurate boundaries in bronchial and alveolar regions, particularly in cases with overlapping pathological features. These visual results further support the quantitative Dice coefficient findings.

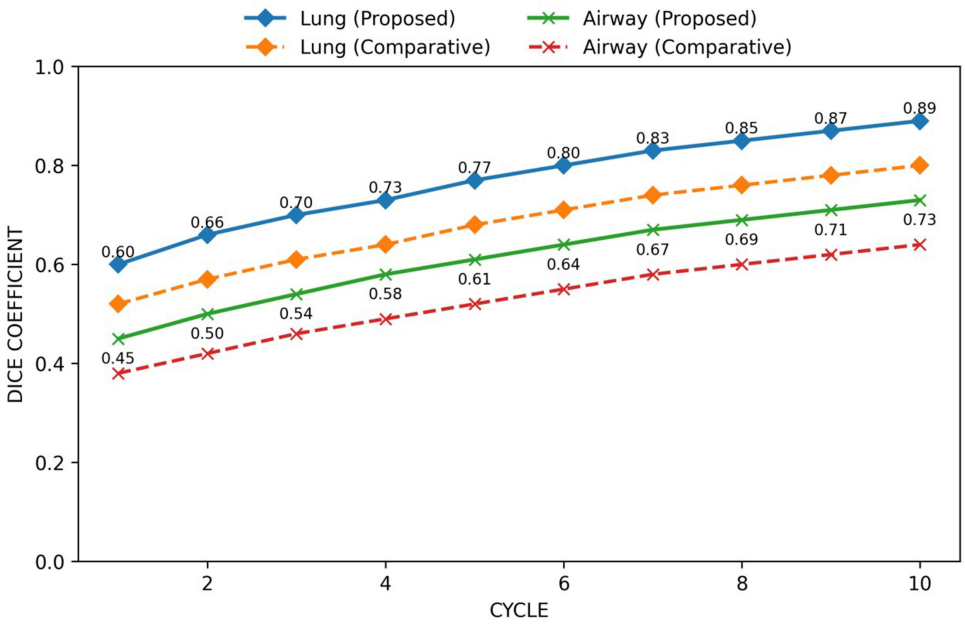

Figure 10 Comparative Dice convergence curves for lung and airway segmentation between the proposed and baseline models.

Dice Analysis Subsection

The proposed method achieved significantly higher Dice values in clinically central structures, including lung parenchyma and bronchus, compared with baseline models ($P < 0.05$). In contrast, improvements in upper-airway structures such as the pharynx and larynx were modest and did not reach statistical significance. Overall, lung parenchyma segmentation yielded higher Dice values than airway-related structures, reflecting the increased boundary complexity of airway anatomy.

Conclusion

ACO patients tend to experience more frequent exacerbations, worse health-related quality of life, and higher healthcare utilization than patients with asthma or COPD alone.[26] With increasing emphasis on precision phenotyping and treatable traits in obstructive airway diseases, improving disease control and stratification in ACO has become an important clinical and research priority. In this study, we explored a deep transfer learning-based CT image segmentation framework to support ACO-related classification as a proof-of-concept approach. Nevertheless, the present evidence is limited to internal evaluation in a single-center cohort, and external validation across multiple institutions and imaging settings is essential before clinical translation.

Deep learning is now a well-established methodology in biomedical research and medical image analysis, with extensive applications in classification and segmentation tasks.[27] U-Net and its variants remain foundational baselines for biomedical image segmentation,[28] and transfer learning has been widely adopted to mitigate limited annotations and domain shift.[29] Consistent with prior biomedical studies illustrating the broad applicability of deep learning beyond

Table 6 Dice Similarity Coefficient (DSC) for Different Anatomical Structures on the Test Set

Structure	Proposed Method	U-Net	nnU-Net	NUS-PSL	PRE-1000C	*P*
Lung parenchyma	0.94±0.02	0.91 ± 0.03	0.92 ± 0.03	0.89 ± 0.04	0.90 ± 0.03	<0.01
Bronchus	0.88±0.04	0.83 ±0.05	0.85 ± 0.05	0.80 ± 0.06	0.82 ± 0.05	0.02
Pharynx	0.79±0.06	0.77 ± 0.07	0.78 ± 0.06	0.75 ± 0.08	0.76 ± 0.07	0.21
Larynx	0.76±0.07	0.74 ± 0.08	0.75 ± 0.07	0.72 ± 0.09	0.73 ± 0.08	0.28

https://doi.org/10.2147/COPD.S578685

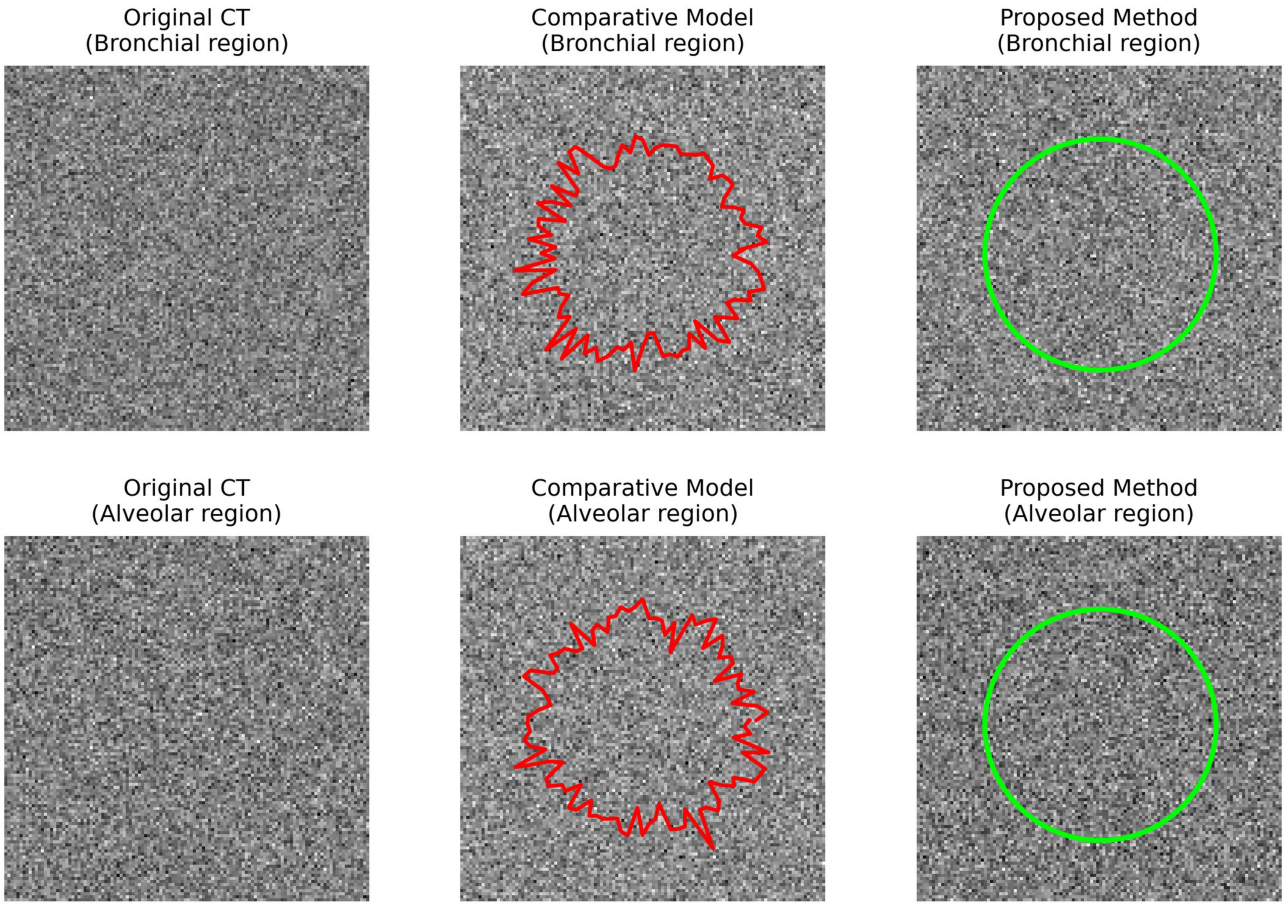

Figure 11 Visual comparison of representative segmentation results. Ground-truth and predicted contours are overlaid on CT slices. Case-level Dice coefficients are annotated on each panel, and zoomed-in regions highlight bronchial and alveolar boundaries.

imaging and perspectives discussing the intersection of deep learning and radiomics,[30,31] our work is positioned within this broader methodological landscape while focusing specifically on segmentation-driven CT analysis for obstructive airway phenotyping.

It should be emphasized that the proposed deep transfer learning–based segmentation model is not designed to replace conventional clinical diagnosis of ACO, which primarily relies on clinical history, spirometry, bronchodilator responsiveness, and inflammatory biomarkers.[32] Instead, it provides complementary structural information derived from CT imaging, which may reflect airway remodeling and parenchymal alterations relevant to different obstructive airway phenotypes.[33] When interpreted in conjunction with clinical symptoms, lung function parameters, and inflammatory biomarkers, such image-based features may support phenotypic characterization and risk stratification, consistent with multimodal assessment in complex airway diseases. Technically, the segmentation framework focuses on airway-adjacent and parenchymal structures, which are closely related to airway remodeling and emphysema/air-trapping patterns on CT.[34,35] The observation that lung parenchyma segmentation achieved higher Dice values than airway-related structures is consistent with the higher boundary complexity and smaller caliber of airway structures and their susceptibility to partial-volume effects. The more continuous boundaries generated by the proposed method may facilitate more reliable extraction of imaging features for downstream classification. Given that ACO is primarily characterized by lower-airway and parenchymal abnormalities, segmentation results for upper-airway structures such as the pharynx and larynx are considered exploratory and are not used to support the primary clinical conclusions of this study.

This study has several limitations. First, the cohort comprised 200 patients from a single center, which may limit representativeness and clinical heterogeneity. Second, no external validation cohort was included; therefore, performance reflects internal evaluation only, and any statements regarding stability or generalizability should remain conservative. Third, robustness analyses

(eg, repeated resampling/cross-validation and sensitivity analyses across acquisition settings) were not performed. Future work will involve multi-center data collection, independent external testing, and reporting in accordance with established medical imaging AI guidelines (eg, CLAIM) and prediction model reporting guidance (eg, TRIPOD+AI).[36,37]

Data Sharing Statement

The imaging dataset used in this study contains patient-related clinical information and is therefore not publicly available due to privacy and ethical restrictions. De-identified derived data (e.g, summary statistics and evaluation outputs) and the annotation protocol can be made available from the corresponding author upon reasonable request and with approval from the institutional ethics committee, in accordance with applicable regulations.

Ethics Statement

Ethical approval was granted by the Ethics Committee of Panyu Maternal and Child Care Service Center of Guangzhou (He Xian Memorial Affiliated Hospital). Informed consent was obtained from all participants.

Acknowledgments

The authors sincerely thank Yanchao Gao for their valuable support and assistance.

Author Contributions

All authors made a significant contribution to the work reported, whether that is in the conception, study design, execution, acquisition of data, analysis and interpretation, or in all these areas; took part in drafting, revising or critically reviewing the article; gave final approval of the version to be published; have agreed on the journal to which the article has been submitted; and agree to be accountable for all aspects of the work.

Funding

This research received no specific grant from any funding agency in the public, commercial, or not-for-profit sectors.

Disclosure

The authors declare no conflicts of interest in this work.

References

1. Addagarla SK, Chakravarthi GK, Anitha P. Real time multi-scale facial mask detection and classification using deep transfer learning techniques. *Int J Adv Trends Comp Sci Eng*. 2020;9(4):4402–4408. doi:10.30534/ijatcse/2020/33942020
2. Wang G, Zuluaga MA, Li W, et al. DeepIGeoS: a deep interactive geodesic framework for medical image segmentation. *IEEE Trans Pattern Anal Machine Intell*. 2019;41(7):1559–1572. doi:10.1109/TPAMI.2018.2840695
3. Yves L, Eric W, Gordon G, et al. Health status measurement instruments in chronic obstructive pulmonary disease. *Canad Resp J*. 2016;4 (3):152–164.
4. Huynh B, Drukker K, Giger M. MO-DE-207B-06: Computer-aided diagnosis of breast ultrasound images using transfer learning from deep convolutional neural networks. *Med Phys*. 2016;43(6):3705. doi:10.1118/1.4957255
5. Gao Y, Mosalam KM. Deep transfer learning for image-based structural damage recognition. *Comput-Aided Civ Infrastruct Eng*. 2018;33 (9):748–768. doi:10.1111/mice.12363
6. Huang Y, Ma X, Liu Y, et al. Effective capacity maximization in beyond 5G vehicular networks: a hybrid deep transfer learning method. *Wireless Commun Mobile Comput*. 2021;2021(4):1–12. doi:10.1155/2021/5792975
7. Li J, Li X, He D, et al. A domain adaptation model for early gear pitting fault diagnosis based on deep transfer learning network. *Proceed Inst Mech Eng Part O*. 2020;234(1):168–182.
8. Cao H, Wang W, Su L, et al. Deep transfer learning for underwater direction of arrival using one vector sensor. *J Acoust Soc Am*. 2021;149 (3):1699–1711. doi:10.1121/10.0003645
9. Lin F, Chen J, Ding G, Jiao Y, Sun J, Wang H. Spectrum prediction based on GAN and deep transfer learning: a cross-band data augmentation framework. *China Commun*. 2021;18(1):18–32. doi:10.23919/JCC.2021.01.002
10. Yuan X, Tao X, Han Z, et al. SegAN: adversarial network with multi-scale L_1 loss for medical image segmentation. *Neuroinformatics*. 2017;16 (6):1–10.
11. Juneja P, Kashyap R. Energy based methods for medical image segmentation. *Int J Comput Appl*. 2016;146(6):22–27. doi:10.5120/ijca2016910808
12. Shen X, Pan H, Chen H. Medical image segmentation algorithm based on one dimensional otsu multiple threshold. *J Jilin Univ*. 2016;54 (2):344–348.

13. Yushkevich PA, Gerig G. ITK-SNAP: An intractive medical image segmentation tool to meet the need for expert-guided segmentation of complex medical images. *IEEE Pulse*. 2017;8(4):54–57. doi:10.1109/MPUL.2017.2701493
14. Zheng H, Zhang Y, Yang L, et al. An annotation sparsification strategy for 3D medical image segmentation via representative selection and self-training. *Proceed AAAI Conf Artif Intell*. 2020;34(4):6925–6932. doi:10.1609/aaai.v34i04.6175
15. Khin T, Raju KS, Sinha GR, et al. Review of optimization methods of medical image segmentation. *Adv Intelligent Syst Computing*. 2020;1090 (1):213–218.
16. Zhang L, Wang X, Yang D, et al. Generalizing deep learning for medical image segmentation to unseen domains via deep stacked transformation. *IEEE Transactions Med Imag*. 2020;39(7):2531–2540. doi:10.1109/TMI.2020.2973595
17. Paul H, Balter MS, Jean B, et al. Canadian practice assessment in chronic obstructive pulmonary disease: respiratory specialist physician perception versus patient reality. *Canad Resp J*. 2016;20(2):97–105.
18. Toledo-Pons N, Cosío BG, Velasco M, et al. Chronic obstructive pulmonary disease in non-smokers. *Arch Bronconeumol*. 2017;53(2):45–46. doi:10.1016/j.arbres.2016.07.013
19. Criner GJ, Chatila WM, Minai OA, et al. Comorbidities in chronic obstructive pulmonary disease. *Arch Bronconeumol*. 2016;52(11):547–548. doi:10.1016/j.arbr.2016.09.005
20. Ameen NM, Mohamed R, Mageed N, et al. The metabolic syndrome in patients with chronic obstructive pulmonary disease. *Egypt J Chest Dis Tuberculosis*. 2016;65(3):593–596. doi:10.1016/j.ejcdt.2016.03.008
21. Zeki AA, Jarjour NN. The asthma–chronic obstructive pulmonary disease overlap syndrome: a new take on an old concept. *Ann Am Thorac Soc*. 2016;13(9):1440–1442. doi:10.1513/AnnalsATS.201606-493ED
22. Aa A, Gfw B, Ds B, et al. Asthma, allergic sensitization and lung function in sickle cell disease - ScienceDirect. *Allergologia et Immunopathologia*. 2020;48(5):450–457. doi:10.1016/j.aller.2019.12.012
23. Gu YL, Jin ML, Ye X. New progress of targeted anti-inflammatory therapeutics in asthma and chronic obstructive lung disease. *Zhonghua jie he he hu xi za zhi*. 2016;39(10):799–802. doi:10.3760/cma.j.issn.1001-0939.2016.10.012
24. Durham AL, Caramori G, Chung KF, et al. Targeted anti-inflammatory therapeutics in asthma and chronic obstructive lung disease. *Transl Res*. 2016;167(1):192–203. doi:10.1016/j.trsl.2015.08.004
25. Urbanic RJ, Saqib SM, Aggarwal K. Using predictive modeling and classification methods for single and overlapping bead laser cladding to understand bead geometry to process parameter relationships. *J Manuf Sci Eng*. 2016;138(5):172–192. doi:10.1115/1.4032117
26. Alshabanat A, Zafari Z, Albanyan O, Dairi M, FitzGerald JM. Asthma and COPD overlap syndrome (ACOS): a systematic review and meta analysis. *PLoS One*. 2015;10(9):e0136065. doi:10.1371/journal.pone.0136065
27. Litjens G, Kooi T, Bejnordi BE, et al. A survey on deep learning in medical image analysis. *Med Image Anal*. 2017;42:60–88. doi:10.1016/j.media.2017.07.005
28. Tashk A, Herp J, Bjørsum-Meyer T, Koulaouzidis A, Nadimi ES. AID-U-net: an innovative deep convolutional architecture for semantic segmentation of biomedical images. *Diagnostics*. 2022(12(12):2952.
29. Parekh VS, Jacobs MA. Deep learning and radiomics in precision medicine. *Expert Rev Precis Med Drug Dev*. 2019;4(2):59–72. doi:10.1080/23808993.2019.1585805
30. Le NQK, Yapp EKY, Nagasundaram N, Chua MCH, Yeh HY. Computational identification of vesicular transport proteins from sequences using deep gated recurrent units architecture. *Comput Struct Biotechnol J*. 2019;17:1245–1254. doi:10.1016/j.csbj.2019.09.005
31. Le NQK. Hematoma expansion prediction: still navigating the intersection of deep learning and radiomics. *Eur Radiol*. 2024;34(5):2905–2907. doi:10.1007/s00330-024-10586-x
32. Dubin S, Patak P, Jung D. Update on asthma management guidelines. *Mo Med*. 2024;121(5):364–367. doi:10.1378/chest.130.1_suppl.4s
33. Moslemi A, Kontogianni K, Brock J, Wood S, Herth F, Kirby M. Differentiating COPD and asthma using quantitative CT imaging and machine learning. *Eur Respir J*. 2022;60(3):2103078. doi:10.1183/13993003.03078-2021
34. Shimizu K, Hasegawa M, Makita H, Nasuhara Y, Konno S, Nishimura M. Comparison of airway remodelling assessed by computed tomography in asthma and COPD. *Respir Med*. 2011;105(9):1275–1283. doi:10.1016/j.rmed.2011.04.007
35. Lu D, Yu H, Chen L, Lin J, Chen S, Huang Y. Differences in the quantitative HRCT characteristics of patients with asthma, COPD and asthma-COPD overlap and their relationships with pulmonary function. *Int J Chron Obstruct Pulmon Dis*. 2024;19:1775–1789. doi:10.2147/COPD.S469956
36. Mongan J, Moy L, Kahn CE Jr. Checklist for artificial intelligence in medical imaging (CLAIM): a guide for authors and reviewers. *Radiol Artif Intell*. 2020;2(2):e200029. doi:10.1148/ryai.2020200029
37. Collins GS, Moons KG, Dhiman P, et al. TRIPOD+AI statement: updated guidance for reporting clinical prediction models that use regression or machine learning methods. *BMJ*. 2024;385. q902. Erratum for: BMJ. 2024,385e078378. doi:10.1136/bmj.q902